Atmosphere-Mediated Superhydrophobicity of Rationally Designed Micro/Nanostructured Surfaces

Atmospheric-Mediated Superhydrophobicity of Rationally Designed Micro/Nanostructured Surfaces

Xiao Yan[1, 2], Zhiyong Huang[2], Soumyadip Sett[1], Junho Oh[1], Hyeongyun Cha[1], Longnan Li[1], Lezhou Feng[1], Yifan Wu[1], Chongyan Zhao[2], Daniel Orejon[5,6*], Feng Chen[2*], Nenad Miljkovic[1,3,4,5*]*

[1]Department of Mechanical Science and Engineering, University of Illinois at Urbana–Champaign, Urbana, IL, 61801, USA
[2]Institute of Nuclear and New Energy Technology, Tsinghua University, Beijing, 100084, China
[3]Department of Electrical and Computer Engineering, University of Illinois at Urbana–Champaign, Urbana, IL, 61801, USA
[4]Frederick Seitz Materials Research Laboratory, University of Illinois at Urbana–Champaign, Urbana, Illinois 61801, USA
[5]International Institute for Carbon Neutral Energy Research (WPI-I2CNER), Kyushu University, 744 Moto-oka, Nishi-ku, Fukuoka, 819-0395, Japan
[6]Institute for Multiscale Thermofluids, School of Engineering, The University of Edinburgh, King's Buildings, Edinburgh, EH9 3FD, United Kingdom

*Authors to whom correspondence should be addressed.

Electronic mail: Xiao Yan: yan-x13@tsinghua.org.cn, Daniel Orejon: d.orejon@ed.ac.uk, Feng Chen: fengchen@tsinghua.edu.cn, Nenad Miljkovic: nmiljkov@illinois.edu

ABSTRACT

Superhydrophobicity has received significant attention over the past three decades owing to its significant potential in self-cleaning and anti-icing surfaces, drag reduction, energy harvesting devices, anti-bacterial coatings, and enhanced heat transfer applications. Superhydrophobicity can be obtained *via* the roughening of an intrinsically hydrophobic surface, the creation of a re-entrant geometry, or by the roughening of a hydrophilic surface followed by a conformal coating of a hydrophobic material. Intrinsically hydrophobic surfaces have poor thermophysical properties such as thermal conductivity, and thus are not suitable for heat transfer applications. Re-entrant geometries, although versatile in applications where droplets are deposited, break down during spatially random nucleation and flood the surface. Chemical functionalization of rough metallic substrates, although promising, is not utilized due to the poor durability of conformal hydrophobic coatings. Here we develop a radically different approach to achieve stable superhydrophobicity. By utilizing laser processing and thermal oxidation of copper (Cu) to create a high surface energy hierarchical copper oxide (CuO), followed by repeatable and passive atmospheric adsorption of hydrophobic volatile organic compounds (VOCs), we show that stable superhydrophobicity with apparent advancing contact angles ≈ 160° and contact angle hysteresis as low as ≈ 20° can be achieved. We exploit the structure length scale and structure geometry dependent VOC adsorption dynamics to rationally design CuO nanowires with enhanced superhydrophobicity. To gain an understanding of the VOC adsorption physics, we utilized X-Ray Photoelectron and Ion Mass Spectroscopy to identify the chemical species deposited on our surfaces in two distinct locations: Urbana, IL, USA and Beijing, China. To test the stability of the atmosphere-mediated superhydrophobic surfaces during heterogeneous nucleation, we used high-speed optical microscopy to demonstrate the occurrence of dropwise condensation and stable coalescence-induced droplet jumping. Our work not only provides rational design guidelines for developing passively-durable superhydrophobic surfaces with excellent flooding-resistance and self-healing capability, but also sheds light on the key role played by the atmosphere in governing wetting.

KEYWORDS: superhydrophobic, volatile organic compounds, coalescence-induced droplet jumping, condensation heat transfer, adsorption, nanostructure, wetting

Superhydrophobicity has received much attention over the past three decades owing to its significant potential in enhancing self-cleaning,[1] drag reduction,[2] liquid transport,[3] anti-corrosion,[4] anti-icing,[5] anti-frosting,[6] and phase change heat transfer.[7] Creating a superhydrophobic surface does not follow a single recipe. Generally, three methods of fabrication exist: i) roughening of an intrinsically hydrophobic substrate,[8] ii) fabrication of a re-entrant roughness geometry,[9] and the most common of all iii) roughening of an intrinsically hydrophilic substrate followed by the conformal deposition of a thin conformal hydrophobic coating.[10] From a fundamental standpoint, each manufacturing approach has its pitfalls, resulting in the lack of utilization of superhydrophobic surfaces in many applications. An example of this is observed in condensation heat transfer, where enhancing the condensation efficiency is paramount for applications ranging from industrial power plants[11] to compact heat pipes.[12]

When water vapor condenses on a hydrophilic substrate, it forms a liquid film growing in thickness along the gravitational direction, termed filmwise condensation. The liquid film significantly decreases the heat transfer due to the low thermal conductivity of the condensate.[13] The key to enhancing heat transfer is efficiently removing the condensate as fast as possible.[14] To enhance removal, researchers more than eight decades ago demonstrated that by coating the condensing surface with a low-surface energy (hydrophobic) promoter, such as a thin polymer layer or self-assembled monolayer (SAM), water condenses into discrete droplets ranging in size from nanometers to millimeters.[15] Termed dropwise condensation, these droplets grow *via* direct condensation and coalescence, and result in rapid shedding *via* gravitational body forces, sweeping other droplets from the surface. The subsequent re-clearing of the surface and re-nucleation makes dropwise condensation up to ten times more efficient than filmwise condensation.[14] Furthermore, the recent combination of surface micro/nanostructure with hydrophobic promoter coatings has

enabled ever-smaller length scales (≈10 μm) of droplet shedding[7,16-20] providing further increases in heat transfer rates *via* coalescence-induced droplet jumping.[7,19]

Promoting lasting dropwise condensation is still an unsolved problem despite considerable effort spanning the 20th century. At a fundamental level, the durability of current promoter coatings provides stable dropwise condensation for hours,[21] not the year timescales required by real-life systems. Re-entrant surfaces break down under condensing conditions due to nucleation between structures and flooding of the intrinsically hydrophilic substrate. The utilization of intrinsically hydrophobic rough substrates is not desirable due to the low characteristic thermal conductivity of most intrinsically hydrophobic materials (< 1W/m·K). Hence, the majority of current condensation applications utilize the innate hydrophilic surface chemistry of high surface energy metal oxides to ensure long-lasting filmwise condensation.

Given the restrictions of conventional superhydrophobic surfaces, researchers have attempted to exploit the "intrinsic" hydrophobicity of inorganic materials with relatively high thermal conductivity. Good water repellency was displayed on noble metals,[22-24] metal oxides,[25,26] rare earth oxides,[27-30] boron nitride,[31,32] and graphene,[33,34] which was initially attributed to the intrinsic low surface energy of the materials.[25,27,30] However, the intrinsic hydrophobicity has been debated,[25,27-30,32] with many studies[22,28,29,35,36] showing adsorption of atmospheric volatile organic compounds (VOCs) playing an important role. The majority of these VOCs are composed of alkanes, olefins, aromatic hydrocarbons, halogenated hydrocarbons and oxygen-containing organic molecules, stemming from the biochemical,[37] industrial,[38] and human processes.[39,40] Although promising, VOC-adsorption-induced hydrophobicity has not garnered much interest as a functionalization technique due to incomplete surface coverage resulting in high contact angle hysteresis,[28] and insufficient understanding of VOC adsorption dynamics.

Here, we elucidate the mechanisms governing VOC adsorption dynamics on micro/nanostructured copper oxide (CuO) surfaces, demonstrating a fourth avenue to achieve atmosphere-mediated superhydrophobicity with low contact angle hysteresis. By rationally designing hierarchical Cu-based metal oxide superhydrophilic substrates tailored to enable efficient adsorption of VOCs from the atmosphere, we demonstrate stable superhydrophobicity approaching advancing contact angles greater than 160° and roll-off angles less than 10° with water. To fabricate the hierarchical substrates, laser processing of smooth Cu sheets was utilized to create a microscale roughness followed by thermal oxidation to grow CuO nanowires conformally on the microscale asperities. To study VOC adsorption dynamics, we utilized time-resolved X-Ray Photoelectron Spectroscopy (XPS) and Time of Flight Secondary Ion Mass Spectroscopy (ToF-SIMS) showing the presence of adsorbed light hydrocarbons containing 2-4 carbon atoms in an aliphatic chain on the intrinsically hydrophilic surfaces. To characterize repeatability, we allowed VOC adsorption to occur in the mid-western United States (Urbana, IL) as well as mainland China (Beijing). Both locations demonstrated atmosphere-mediated superhydrophobicity with Chinese samples having higher saturated apparent advancing contact angles ($\approx 164 \pm 1°$) when compared to the continental United States ($\approx 159 \pm 1°$) owing to the higher atmospheric concentration of VOCs. Furthermore, we show that superhydrophobicity can be enhanced by exposing the samples to VOC-rich environments and activating them *via* plasma treatment prior to adsorption. To demonstrate the benefit of our hierarchical surfaces, we utilized high-speed optical microscopy imaging of atmospheric water vapor condensation showing dropwise condensation and the occurrence of stable coalescence-induced droplet jumping. Durability quantification using thermal annealing to 200°C, mechanical abrasion, self-cleaning, pure water vapor condensation, 100°C steam condensation, and exposure to the outside sunlight

environment revealed the capacity for self-healing of atmosphere-mediated superhydrophobic surfaces when compared to classical hydrophobic coating methods. Benchmarking the VOC adsorption on CuO nanowires with chemical-oxidation-based CuO nanoblade surfaces, Al micro and nanostructures, and Si nanostructures revealed a delicate interplay between surface chemistry and structure to minimize contact angle hysteresis and achieve stable droplet jumping, with CuO nanoblades becoming superhydrophobic ($\theta_a^{app} \approx 167 \pm 2°$), while showing no droplet jumping after VOC saturation. This work not only to develops a manufacturing method to achieve durable superhydrophobic surfaces through passive VOC healing, but also establishes design guidelines for the fabrication of nanoengineered surfaces for efficient atmospheric-mediated functionalization with minimal contact angle hysteresis.

RESULTS

Non-Flaking CuO Nanowire Surfaces with Controllable Micro/Nanostructures

Laser ablation followed by thermal oxidation[41,42] was used to fabricate micro/nanostructures on Cu substrates (99.9% purity) (Figure 1a). Specifically, we first utilized a picosecond laser (PX100 intelliSCANSe14, Edgewave, Germany) to etch microstructures (Figure 1b), which acted as skeletons supporting the subsequent nano-features. Owing to the Gaussian distribution of the laser power intensity,[43] hill-like microstructures (Figure 1c-f) were formed. After laser ablation, we placed the samples into an atmospheric furnace (SK-1200, Zhonghuan, China) to oxidize in quiescent air at 480°C for 2 hours (seen Methods for further fabrication details). During thermal oxidation, CuO nanowires grew perpendicular to the laser processed features (Figure 1g-j). The length, thickness, and number density of nanowires was dependent on the oxidation temperature and duration.[41,44] The nanowires in the hill ridge areas had lengths $h \approx$ 5-10 μm (Figure 1l),

diameters $d \approx 200$ nm (Figure 1k and 1l), and center-to-center spacing $l \approx 0.6$ μm (Figure 1k), resulting in an estimated roughness of $r = 1 + \pi dh/l^2 \approx$ 10-18 and an upper bound of solid fraction $\varphi = \pi d^2/4l^2 \approx 0.09$. Note, the real solid fraction was most likely smaller than theoretically estimated due to the non-uniform nanowire spacing and sharp tip nanowire termination.

Although nanowires alone can provide the nanoscale roughness indispensable for superhydrophobicity, incorporating microscale features by laser processing was paramount to the rational design of the surface. The microscale features help release the residual stress during oxidation and enhance the adhesion of the oxide layer to the substrate,[45,46] reducing chances of flaking (Section S2, Figure S1, Supporting Information).[47,48] To demonstrate the design versatility and scalability of the laser ablation-thermal oxidation method, various morphologies were fabricated (Figure 2). All surfaces shown in Figure 2 demonstrated atmosphere-mediated superhydrophobicity (Section S3, Figure S3, Supporting Information), with excellent non-wetting properties insensitive to microscale morphology. To simplify the experimental design space, the hierarchical CuO nanowire surfaces with hill-like structures (Figure 2d-f) were used for all studies herein.

VOC-Adsorption-Induced Superhydrophobicity

The synthesized hierarchical CuO nanowire surfaces were exposed to the atmosphere by placing samples top-up in glass vials with no lid, exposing them to the laboratory environment. The laboratory was located in Urbana (40°06' N, 88°13' W), Illinois, USA and exposure was done during the months from May to August of 2017. During exposure, the samples were placed in a low-traffic area of the laboratory to minimize convective air currents. Hydrophobicity was monitored by measuring the contact angles during a period spanning 3 months from sample

fabrication. The advancing and receding contact angles were characterized *via* microgoniometry, crucial to obtaining high fidelity while avoiding deposition-mediated Cassie-to-Wenzel transitions (see Methods).

Interestingly, the water droplet advancing contact angle of the hierarchical CuO nanowire surfaces gradually increased with exposure time (Figure 3a). The surface immediately after thermal oxidation was superhydrophilic with an advancing contact angle of 0°, confirming the intrinsic hydrophilicity of CuO[7] governed by the presence of hydroxyl groups at the surface which interact strongly with polar water molecules. However, after a three-week atmospheric exposure to the laboratory atmosphere, the apparent advancing contact angle eventually reached 159 ± 1°, with a receding contact angle of 112 ± 8°, and water droplet roll-off angle of 26 ± 5° (see Methods).

To examine the mechanism of increased hydrophobicity, we analyzed the temporally varying surface chemistry using X-Ray Photoelectron Spectroscopy (XPS) (see Figure 4a-c and Methods). Broad energy scans (Figure 4a) showed the presence of copper Cu, oxygen O and carbon C on the sample surfaces. High-resolution spectra of C 1s and O 1s revealed that the content of C and O increased significantly during surface exposure to the ambient. Specifically, the atomic ratio of C 1s to Cu 2p (C/Cu), indicative of the total amount of the adsorbed organic matter, increased by ≈ 500% after 104 days of atmospheric exposure (see Section S6, Supporting Information). Similarly, the atomic ratio of O 1s to Cu 2p (O/Cu) increased by ≈ 50%. Correspondingly, the C-C (or C-H), C-O, and C=O bond content normalized with Cu 2p content also increased with differing amplitudes. Analyzing the concentration of C-C (or C-H), C-O, and C=O bonds relative to the total C 1s content revealed that C-C (or C-H) was the dominant component of the adsorbate with a relative concentration of ≈ 70% upon surface exposure for 104 days. The nonpolar C-C (or C-H) bond is responsible for the hydrophobicity of the adsorbate,[49-51] while polar C-O and C=O

incur hydrophilicity.[52] Indeed, as the C-C (or C-H) content increased, the surface experienced an increase of contact angle from 0º to ≈ 159º (Figure 3a).

Further surface analysis using Time of Flight Secondary Ion Mass Spectroscopy (ToF-SIMS) (see Methods) also revealed that the increase in carbon content was due to the adsorption of light hydrocarbons, *i.e.*, short chain hydrocarbons, on the hierarchical CuO nanowire surface. Compared with the clean surface at t = 0 day (Figure 4d), the hierarchical CuO nanowire surface exposed to the laboratory atmosphere for 104 days (Figure 4e) showed increased signals for positive ions such as C_2H_3, C_2H_5, C_3H_5, and C_3H_7 (Section S6, Supporting Information). For negative ions, distinctively high counts of H, OH, OH_3 ions were observed (Figure 4f and g). The increasing hydrocarbon content detected *via* ToF-SIMS was in accordance with the increasing C-C (or C-H) components measured *via* XPS, confirming the more relevant role of non-polar hydrocarbon groups responsible for the surface hydrophobicity.[49-51]

In addition to XPS and ToF-SIMS, Attenuated Total Reflection Infrared Spectroscopy (ATR-IR) as well as Raman Spectroscopy was conducted on the samples with limited success due to the weak VOC signal-to-noise ratio stemming from the high penetration depth of these methods (Section S6, Supporting Information).

To confirm that the atmosphere-mediated superhydrophobicity was universal at the global scale, we repeated our experiments in Beijing, China (39°59' N, 116°19' E) during the months from September 2016 to November 2016. Surprisingly, the hierarchical CuO nanowire samples showed better superhydrophobicity, reaching apparent advancing contact angles of 164 ± 1°, with receding contact angles of 123 ± 4°, and water droplet roll-off angles of 9 ± 1°. Furthermore, the samples in China reached the saturation contact angle in less than one week of laboratory exposure, whereas it took approximately three weeks to reach saturation in the USA (Figure 3a). The improved

superhydrophobicity and accelerated adsorption stemmed from the higher levels of VOCs in Beijing[38,53] when compared to Urbana (Section S4, Supporting Information).

Atmospheric-Mediated Self-Healing and Abrasion Robustness

The differing contact angle dynamics on the hierarchical CuO nanowire samples indicated the relevant role of atmosphere on adsorption dynamics. To further study the effect of environment, we intentionally exposed the hierarchical CuO nanowire surface to a machine shop (MS) atmosphere in Urbana, where the air was rich in VOCs originating from petroleum-based lubricants used for metal processing. Indeed, ToF-SIMS characterization showed the presence of heavier complex negative ions ($C_xH_yO_zN_m$) on the MS exposed CuO nanowire samples (Section S4, Figure S7, Supporting Information) when compared to cleaned samples or the samples exposed to the lab atmosphere. The MS exposed CuO nanowire samples were initially superhydrophilic. As the exposure time increased, the apparent advancing contact angle increased, plateauing at ≈ 160° after ≈ 6 days, much faster compared with the three weeks required for the sample exposed to laboratory atmosphere (Figure 3b). As further confirmation of the role of the atmosphere, a clean the hierarchical CuO nanowire sample was stored in a glass container with a lid on top, isolating it from the ambient air. The sealed sample experienced slower advancing contact angle increase (Figure 3b) due to VOC depletion from the contained air (see Methods).

To study the effect of surface structure, and to ensure that hierarchical CuO nanowires were not contributing to the superhydrophobicity due to their particular structure, we conducted additional tests on CuO nanoengineered surfaces[7] having characteristic nanoblade-like structures differing significantly from the hierarchical CuO nanowires. The CuO nanoblade surfaces were fabricated with a chemical-oxidation method (see Methods). As with the hierarchical CuO nanowires, the CuO nanoblade samples exposed to the MS atmosphere and isolated in a container

showed the highest and lowest advancing contact angle saturations, respectively (Figure 3c). The distinct contact angle growth trends on the hierarchical CuO nanowire and nanoblade surfaces was attributed to the different surface structure geometries and length scales. Unlike the single-tier roughness CuO nanoblades, the additional microscale features on the hierarchical CuO nanowire surfaces play an important role in determining the time-dependent advancing contact angle through their governance of the surface roughness and solid fraction.

To study the role of surface hydroxylation state, we conducted additional experiments by modifying the hierarchical CuO nanowire surface with air plasma prior to atmospheric exposure. Air plasma cleaning (see Methods) of the samples for 3-5 min prior to laboratory exposure resulted in accelerated growth of the apparent advancing contact angles (Figure 3b), exceeding ≈ 150° after 4 days. The non-plasma-cleaned hierarchical CuO nanowire sample required ≈ 17 days to reach an apparent advancing contact angle of ≈ 150°. Furthermore, the saturation apparent advancing/receding contact angles of the same hierarchical CuO nanowire surface after plasma modification increased from 156 ± 2°/103 ± 4º to 162 ± 2°/117 ± 6º.

In order to confirm the efficacy of the air plasma treatment, we subjected the CuO nanoblade surfaces to the same plasma cleaning. On the CuO nanoblade surfaces the apparent advancing contact angle increase accelerated in a similar fashion (Figure 3c). After a 29-day atmospheric exposure, apparent advancing contact angles as high as 168 ± 2° were observed. The accelerated VOC deposition for both hierarchical CuO nanowire and nanoblade surfaces was likely due to activation of the surfaces after air plasma modification,[54,55] resulting in a higher surface coverage of hydroxyl groups. The transition from superhydrophilic to superhydrophobic after plasma treatment was repeatable (see Section S5, Figure S8, Supporting Information), demonstrating the

self-healing nature of the surface due to the permanent and reliable source of VOCs in the ambient air.

To further demonstrate atmosphere-mediated self-healing, we exposed the hierarchical CuO nanowire surfaces to outdoor conditions in Urbana, IL (see Section 7, Supporting Information), as well as controlled thermal annealing (up to 200°C, see Section 7, Supporting Information). Although exposure to sunlight and thermal annealing resulted in partially desorption of the VOCs, resulting in decreased hydrophobicity, subsequent atmospheric exposure of the degraded surfaces led to the recovery of the superhydrophobicity (Section S7, Figures S12 and S16, Supporting Information).

In addition to atmospheric-mediated self-healing, the hill-like microscale features of our hierarchical CuO surfaces enabled good abrasion resistance *via* sacrificial approaches. Under the protection of the hill-like microstructures, nanowires in the ridge and valley areas could survive mechanical damage, making the surface more robust to abrasive wear (Section S7, Figure S15, Supporting Information). The apparent advancing/receding contact angles on the hierarchical CuO nanowire and single-tier CuO nanoblade surfaces after four abrasion cycles reduced to 158 ± 7°/89 ± 10º and 122 ± 10°/0 ± 5º, respectively.

Stable Dropwise Condensation and Coalescence-Induced Droplet Jumping

In order to test the robustness of the atmospheric-mediated superhydrophobicity, we performed condensation experiments on the hierarchical CuO nanowire and nanoblade surfaces in ambient conditions (see Methods). The hierarchical CuO nanowire surfaces tested here showed stable dropwise condensation for 10 cumulative condensation-evaporation cycles, with each cycle lasting ≈20 min. Unlike single-tier microstructured surfaces on which condensate can penetrate into

micro-cavities and result in loss of water repellency,[56,57] the hierarchical CuO nanowire surface showed excellent resistance to flooding at reduced supersaturations.[58] By shifting the focal plane of the microscope downwards beneath the droplet center-of-mass (see Methods), we were able to clearly observe a number of small droplets growing beneath larger droplets residing on the microstructure tops (Figure 5a and Video S1) in the suspended or partially wetting Cassie-Baxter state.[59] As the shaded small droplets (< 10 μm) grew in size, they were eventually absorbed by the larger droplets (~ 100 μm) residing on top, initiating re-nucleation at the same location. More interesting was the observation of stable coalescence-induced droplet jumping[7,19] of droplet pairs and multiple droplets (Figure 5b, see Video S2). Droplet jumping was further confirmed during pure vapor condensation in a vacuum chamber at saturated vapor pressure of ≈2.7 kPa (Figure S20a, see Video S3). To further study the observed jumping process, we utilized a piezoelectric dispenser to deposit two equally sized droplets having diameters of 156 ± 1 μm, allowing them to coalesce and observe the jumping process with a high-speed camera from the side (Figure 5c) (see Methods). During the coalescence process (see Video S4), the hierarchical CuO nanowire surface showed low pinning, resulting in a detachment velocity in the surface-normal direction of 0.17 ± 0.02 m/s (Section S1, Supporting Information) that agreed well with inertial-capillary scaling.[19,60]

To elucidate the role of surface structures on the atmospheric-mediated superhydrophobicity during water vapor condensation, we analyzed the condensate droplet growth and coalescence dynamics on the CuO nanoblade and CuO nanowire surfaces, both of which had saturated apparent advancing contact angles for water $\theta_a^{app} > 160^o$ arising from the VOC adsorption. To ensure a fair comparison and to eliminate the interference of microstructures, we enlarged the microstructure intervals of the hill-like structures to $I = 200$ μm on the CuO nanowire surface, thus allowing us

to isolate the vital role played by the nanostructures in the initial stage of droplet growth.[57] Consistent with dropwise condensation on the hierarchical nanowire surface (Figure 5a and 5b), condensate droplets on the CuO nanowire surface with sparse micro-features (Figure 6a) showed excellent mobility after coalescence, as evidenced by the spherical morphology of the merged droplets and by the stable coalescence-induced jumping of sub-10-μm droplet pairs (Figure 6b). In contrast, droplets on the CuO nanoblade surface (Figure 6c) spread laterally as they grew and coalesced, showing large contact angle hysteresis that hindered the depinning of the contact line of the merging droplets, resulting in irregular droplet shape morphologies and eventual flooding of the surface (Figure 6d).

The distinct condensate droplet behavior on the atmospheric-mediated CuO nanowire and CuO nanoblade surfaces can be explained by the different shape of the surface nano-structures, which not only dictates the droplet wetting behavior, but also influences the VOC adsorption dynamics. For the CuO nanowire surface, the dense and slender nanowires lead to a large roughness factor $r \approx$ 10-18 with relatively small solid fraction $\varphi < 0.09$. For the CuO nanoblade surface, r and φ have been shown to be ≈ 10 and ≈ 0.04,[61] respectively. Correspondingly, the critical intrinsic contact angle, $\theta_c = \cos^{-1}[(\varphi - 1)/(r - \varphi)]$,[62] is ≈ 93-96º and ≈ 96º for the CuO nanowire and CuO nanoblade surfaces, respectively, showing little difference. However, the observed small receding contact angle (≈ 0º) and large roll-off angle (> 90º) of droplets on the CuO nanoblade surfaces suggests the petal effect[63] or Wenzel state.[64] On the CuO nanowire surfaces, droplets nucleate and grow in the Cassie-Baxter state, which was evidenced by the relatively large receding contact angle (145 ± 6º) and small roll-off angle (< 10º). Rather than the surface features alone, the structure-mediated surface chemistry along with the surface features governs the different observed wetting regimes. Smaller scale nanostructures (nanoparticles or

nanotubes) have enhanced adsorption due to an increase in surface molar energy as particle size decreases and curvature increases.[65,66] From a thermodynamic perspective, in order to decrease the total free energy, smaller particles with increased free energy are more prone to adsorb molecules onto their surfaces when compared to their larger counterparts.[32,65] Analogously, the CuO nanowires with small diameters (~100 nm) were observed to have higher VOC adsorption compared to CuO nanoblades, resulting in lower contact angle hysteresis. Indeed, the hierarchical CuO nanowire surface retained good hydrophobicity (θ_a^{app} = 156 ± 1º, θ_r^{app} = 99 ± 9º) even after acetone, isopropanol, ethanol, and deionized (DI) water cleaning (see Methods), while for the CuO nanoblade surface, θ_a^{app} and θ_r^{app} reduced to 40 ± 5º and ≈ 0º, respectively.

In addition, on the CuO nanowire surfaces, multiple droplets were observed to nucleate and grow on the tips of single nanowires (Figure 6e-g, see Video S5). Due to the very limited droplet-surface contact area, the droplet expanded spherically (t = 0 - 7.7 s, Figure 6f) until reaching neighboring nanowires (t = 46.8 s, Figure 6f). The nucleation preference on the nanowire tips may arise due to the geometry of the nanowire comprising bicrystal CuO.[67] In the near-tip region, there exists a characteristic intersecting step concave (Figure 6e), which reduces the heterogeneous nucleation energy barrier.[68,69] We note that the observed nanoscale droplets on the tips of CuO nanowires resulted from heterogeneous nucleation of water vapor (Video S5), and not due to mist deposition on the sample. Furthermore, the long and dense nanowires could potentially slow vapor diffusion within the roughness thus reducing the probability for nucleation at the base of the CuO nanowires.[70,71] Distinct from droplets nucleating within the roughness of the CuO nanoblade surface (Figure 6d), droplets forming on top of the nanostructures tended to grow in the Cassie-Baxter regime with ultra-low surface adhesion and minimum contact line pinning.

The failure to achieve ideal superhydrophobicity with low contact angle hysteresis on the atmospheric-mediated CuO nanoblade surfaces during condensation indicates that the adsorbed VOCs were not as effective as conformal synthetic hydrophobic coatings, which have been shown to enable frequent coalescence-induced droplet jumping.[7] The failure most likely resulted from the non-conformal deposition of VOCs onto the surface due to lack of affinity given the structure-geometry-dependent surface energy. In addition to CuO nanoblades, condensation-induced flooding of the VOC-saturated laser-ablated micro/nanostructured Cu surface was observed in spite of the demonstrated water repellency towards to deposited sessile droplets ($\theta_a^{app} \approx 155^o$, Section S8, Figure S25a-c, Supporting Information). The flooding of Cu micro/nanostructures highlights the importance of CuO nanowires for creating flood-resistant atmosphere-mediated superhydrophobicity. Given the relatively large contact angle hysteresis ($\approx 20^o$) and $\approx$ 10 μm critical jumping droplet radius (Figure 6b), we anticipate room for improvement in the hierarchical CuO nanowire design[72] in order to achieve further reduction of contact angle hysteresis.

As a last test of durability in higher humidity conditions ($\Phi \geq 96\%$), we conducted additional experiments by exposing the vertically-oriented surfaces to the continuous fog flow (Section S7, Supporting Information). The experiments showed that the hierarchical CuO nanowire surface maintained frequent droplet shedding during the tests lasting ≈ 10 hours (Figure S14). In contrast, the laser-processed micro/nanostructured Cu surface (same fabrication as the hierarchical CuO nanowire surfaces but without thermal oxidation step), with initial hydrophobicity (see Figure S25a-c) transitioned to hydrophilic after ≈ 2 hours, further confirming the higher affinity of VOCs to CuO nanowires when compared to the laser-processed micro/nanostructured Cu. Furthermore, additional experiments exposing the CuO nanowire surface to ≈100°C steam for 110 hours

demonstrated both robustness and self-healing (see Figure S24 and Section S7 in the Supporting Information).

To confirm the droplet-jumping induced self-cleaning capability towards dust contaminants,[1] we visualized droplet jumping dynamics on particle-laden samples. Poly(Methyl Methacrylate) PMMAS particles (≈ 50 μm diameter) were placed on a VOC-saturated surface next to two water droplets having ≈ 30 μm radii. Upon coalescence, the particle was removed from the surface demonstrating self-cleaning (Section S7, Figure S17, Supporting Information).

DISCUSSION

The degree of atmosphere-mediated hydrophobicity and VOC affinity to a surface is dependent on both the intrinsic material, the structure geometry as well as the structure length scale. To examine the effects of surface material and structure geometry on VOC-adsorption, we conducted additional atmospheric exposure experiments on smooth silicon wafers (Si), nanostructured Si (black Si), smooth aluminum (Al), nanostructured Al, micro/nanostructured Al, smooth Cu, smooth CuO, and laser-ablated micro/nanostructured Cu (without CuO nanowires). For surface fabrication and characterization see Section S5 of the Supporting Information. All surfaces exposed to the laboratory environment (Urbana, IL) for 7 weeks showed a temporally dependent increase in advancing contact angle except for the micro/nanostructured Al and nanostructured Si samples. Specifically, the smooth Cu and CuO surfaces transitioned from hydrophilic to hydrophobic ($\theta_a^{app} > 90^o$) after 5-days of atmospheric exposure. The smooth Al and Si surfaces failed to become hydrophobic ($\theta_a^{app} < 90^o$), resulting in the superhydrophilicity ($\theta_a^{app} \approx 0^o$) of their micro or nanostructured counterparts in accordance with the Wenzel equation.[64] The failure to achieve superhydrophobicity on the Al and Si surfaces highlights the significance of the intrinsic

material on atmosphere-mediated hydrophobicity and demonstrates the utility of CuO as an optimal material having intrinsically higher affinity to VOC molecules.

To interpret the atmospheric exposure results and to evaluate the role of surface structure on atmosphere-mediated hydrophobicity, we developed a model combining adsorption kinetics and wetting theory (Section S9, Supporting Information). Adsorption kinetics, which are a function of the surface intrinsic properties such as density of active adsorption sites, density of hydroxyl groups,[73] and surface-adsorbate interaction strength, govern VOC surface coverage and thus the evolution and upper limit of contact angle on atmospheric exposed surfaces. By combining our VOC adsorption model with the Wenzel and Cassie-Baxter equations,[59,64] we predicted time-dependent apparent advancing contact angles. The model showed that structured Al and Si surfaces could not achieve hydrophobicity due to the low saturated advancing contact angle on the smooth surfaces, in agreement with the experimental results. Furthermore, the model predicted a higher growth rate during the initial stage of the apparent advancing contact angle on the hierarchical CuO nanowire surface compared to the single-tier CuO nanoblade surface, in agreement with the experimental results as observed in Figure 3b and c (Figure S27, Supporting Information).

The exposure experiments and analytical model provide a guideline for the optimization of the atmosphere-mediated superhydrophobic surfaces. An optimal surface should not only have a high saturated contact angle (> 160º), but also the timescale for the surface to reach saturation should be small enough to enable rapid self-healing. The rational selection of the substrate materials (CuO rather than Cu, Al, or Si), surface modification techniques (plasma treatment to increase the hydroxyl group density), exposure to a VOC-rich environment (industrialized regions), and surface structure design (hierarchical structures with highly curved nanotextures to enhance the VOC adsorption) are key to achieving ideal atmosphere-mediated superhydrophobicity.

Unlike the traditional approaches to achieve an extended durability of hydrophobicity, which include increasing coating-substrate adhesion,[7,21] coating thickness,[74] or abrasion resistance,[75] the durability of atmosphere-mediated superhydrophobic surfaces is based on self-healing of the thin VOC coating through re-adsorption from the surrounding atmosphere. Although atmospheric exposure of surfaces may not always be possible, VOCs have been shown to exist in ultraclean and ultrahigh vacuum conditions,[76] potentially enabling atmosphere-mediated superhydrophobicity and self-healing in reduced pressure environments.

In spite of our enhanced understanding of atmospheric-mediated hydrophobicity on our metal oxides, the adsorption mechanism (*i.e.*, chemisorption or physisorption) of airborne VOCs was challenging to verify and remains in open debate.[50,51,77] Physical adsorption involves the formation of multiple molecular layers, while chemisorption is characterized by the formation of a monolayer. Furthermore, physical adsorption may take place on the top of a chemisorbed monolayer at long timescales, as hypothesized to be the mechanism here. Our hypothesis is supported by the observed decrease of hydrophobicity after organic solvent cleaning (desorption of physically adsorbed VOC top layers), the relatively long timescales (~ weeks) for VOC adsorption (physical adsorption of multiple monolayers), the relatively good durability to UV ray exposure from the sun (chemical adsorption of VOCs at the CuO interface), and droplet jumping during steam condensation. Furthermore, the variety of VOC molecules present in the atmosphere makes the direct identification of a single adsorption mechanism difficult, as polar compounds such as ketones or aldehydes have been shown to undergo strong adsorption to metal oxide substrates.

To gain a better understanding of the nature of VOC adsorption, we closely examined the chemical state of Cu by XPS. No significant changes of the Cu 2p and/or Cu 2p satellite peaks, Cu 3p, Cu LMM, and Cu LMM2 spectra were observed when comparing oxygen plasma cleaned and

exposed hierarchical CuO nanowire surfaces (Section S6, Figure S10, Supporting Information). Thus, the increasing oxygen content on the surface most likely came from the physical adsorption of oxygen and/or from the oxygen present in the VOCs adsorbed as confirmed *via* ToF-SIMS (Figure 4g). Furthermore, as shown in the XPS data of Figure 4c, we failed to observe an increase of O-C=O bonds on the exposed hierarchical CuO nanowire surfaces, which has been regarded as the evidence of chemical bonding between surface hydroxyl groups and the adsorbate.[50] Recently, a study on TiO_2 surfaces showed that self-assembled carboxylate monolayers form on the surface with high affinity *via* bidentate binding.[49] However, chemisorption remains to be experimentally verified on our CuO nanowires. Given the challenge in identifying physical or chemical bonding, further systematic investigation is needed *via* techniques including scanning tunneling microscopy (STM) in well-controlled environments.[49]

Although studied here for Cu-based, Al-based, and Si-based nanostructures, in the future, it would be interesting to conduct further experiments on ZnO, TiO_2, and Fe_2O_3 nanowires having similar length scale and geometry to examine the dependence of VOC-adsorption dynamics on the structure-coupled surface energy. Furthermore, the material and processing dependent role of hydroxyl group density on VOC adsorption remains to be fully understood, specifically in relation to the apparent advancing and receding contact angles. Computational studies utilizing accelerated molecular dynamics, enhanced sampling, and first principle methods are needed to develop a thorough understanding of VOC-surface affinity and interaction. In addition, although partially elucidated here, the exact species of VOCs contributing to surface hydrophobicity and their sources remain to be identified. Besides VOCs from industrial pollution and biochemical processes, VOCs released by volatile chemical products (VCPs) have been shown to contribute 39-62% of the petrochemical VOCs in the US.[39]

The findings reported here have important implications toward the potential development or long lasting functional coatings. The VOC adsorption mechanism shows that the effects of the surface structure and the nature of the material play an important role on the final wetting state. For systems that operate in ambient conditions such as suitably structured stationary and mobile air-side heat exchangers, atmospheric water harvesters, and non-condensation related applications for drag reduction, anti-biofouling, water shedding, and self-cleaning, VOCs have the potential to act as a replenishing mechanism to obtain durable superhydrophobicity. Furthermore, the results presented here have important implications for past and future studies on surface energy and wetting. The use of goniometry and droplet deposition to study wettability of surfaces has been widely utilized for decades. The VOC adsorption mechanism shown here casts doubt on the validity of interpretation of previous experimental wetting data for surfaces exposed to the atmosphere for considerable times.[78] By elucidating better understanding of the interactions between VOCs and substrates, the present work presents a promising method for exploiting volatile "pollutants" to achieve scalable, robust, self-healing, and long-lasting superhydrophobicity without the need for organosilane or polymeric coatings.

CONCLUSIONS

In summary, through structure-coupled adsorption of airborne VOCs, we demonstrated superhydrophobicity of rationally designed CuO nanowire surfaces, capable of promoting stable coalescence-induced droplet jumping condensation without the need for a polymeric hydrophobic coating. Exposed to the ambient atmosphere, the nanowire surface transitioned from superhydrophilic to superhydrophobic with a saturation apparent advancing contact angle of $\approx 160°$, enabling dropwise condensation and further coalescence induced droplet jumping. The

saturation timescale is ≈3 weeks in laboratory atmospheres encountered in the mid-western USA, significantly accelerated when exposed to VOC-rich industrial environments or activated with air plasma. XPS and ToF-SIMS results showed the presence of light VOCs consisting of 2-4 carbons that are responsible for the superhydrophobicity. The repeated experiments in Beijing, China indicated that the VOC-adsorption mechanism is global. Examination of the role of surface structures in the VOC-adsorption-induced hydrophobicity revealed that large roughness and presence of microstructures embodied with nanostructures with large curvatures is critical to achieving and retaining superhydrophobicity under condensation conditions. The atmosphere-mediated superhydrophobicity developed here stands to not only reduce fabrication costs and simplify manufacturing, but also to enable the self-healing of the adsorbate coatings and extend the durability of superhydrophobicity due to dynamic adsorption of the VOCs, which are ubiquitous in the global atmosphere.

METHODS

Fabrication

A laser ablation and thermal oxidation strategy[42,79] was adopted to fabricate the hierarchical CuO nanowire surfaces (Figure 1, 2, 3a, 3b, 5, 6a, 6b, and 6e-6g). First, finely polished Cu (99.9% purity, RMS roughness ≈ 10 nm, Section S3, Figure S6, Supporting Information) plates were ultrasonically cleaned with acetone for 5 min and rinsed with ethanol, isopropanol, and DI water and dried with nitrogen. Then, microstructures on the Cu substrate were fabricated using an ultra-short picosecond laser (PX100 intelliSCANSe14, Edgewave) system to ablate the surface. The central wavelength, repetition rate, maximum (100%) power of the laser pulse was 1064 nm, 597.44 kHz, and 65.4 W, respectively. The scanning trajectory of the laser beam was

programmable and the scanning was repeated 30 times at a velocity of 3 m/s. A 100-mm field lens was used to focus the laser beam with a laser spot diameter of ≈ 30 μm. After laser processing, to grow nanowires on the laser-ablated surfaces, samples were placed in a tube furnace (SK-1200, Zhonghuan, China). The furnace was programmed to heat up with a temperature ramp rate of 3°C/min and then stabilized at 480 ± 5 °C for 2 hours. The quartz tube of the furnace was open to the laboratory atmosphere, leaving the samples to oxidize in stationary air. After the thermal treatment, the furnace was switched off and the samples were taken out once the furnace temperature dropped below 30 ºC. To provide further guidelines for the fabrication of non-flaking CuO nanowires on the Cu plate, we developed a phase map in terms of thermal oxidation temperature and microstructure length scale based on our surface fabrication experiments (Section S2 and Figure S1 of the Supporting Information).

The CuO nanoblade surface (Figure 3c, 6c and 6d) was fabricated following a previously reported chemical-oxidation method.[7] The mirror-finished Cu plates were first cleaned following the same procedures as the hierarchical surfaces. To remove the native oxide, the samples were immersed in hydrochloric acid solution (HCl, 2 M) for 30 s, and then rinsed with DI water and dried with clean nitrogen. To synthesize CuO nanoblade-like structures, the cleaned samples were then immersed into a hot (96 ± 3 °C) alkaline solution composed of $NaClO_2$, NaOH, $Na_3PO_4 \cdot 12H_2O$, and DI water (3.75:5:10:100 wt. %). The oxidation process lasted ≈ 10 min, after which the samples were again rinsed with DI water and dried with clean nitrogen.

To render the synthesized CuO nanowire and CuO nanoblade surfaces superhydrophobic, the samples were placed top-up in glass vials and exposed to the ambient air (in Urbana, air temperature $T_a \approx 23 \pm 0.5$ °C and relative humidity $\Phi = 50 \pm 5\%$; In Beijing, $T_a \approx 21 \pm 1$ °C and relative humidity $\Phi = 30 \pm 5\%$) in the laboratory (CuO nanowire samples in Figure 3a and 3b) or

machine shop (CuO nanowire and CuO nanoblade samples in Figure 3b and 3c). During the exposure, the samples were placed in a low-traffic area to minimize convective air currents. To isolate the sample from the ambient air, the CuO nanoblade sample (in Figure 3c) was stored top-up in a petri dish (Fisher Scientific) with a diameter of 35 mm and height of 15 mm. The petri dish was covered with the lid and sealed with plastic wrap to avoid direct exchange of air within the sample container with the outside atmosphere. The sealed petri dish was placed in the laboratory environment. The number of contact angle measurements was minimized to 3 per sample to reduce the exposure of the sample to the ambient air.

Characterization

Water contact angles of the CuO nanowire and CuO nanoblade surfaces were measured using a piezoelectric micro-goniometer (MCA-3, Kyowa Interface Science, Japan) with voltage and frequency control. To measure the advancing contact angle, monodisperse water droplets with diameters ranging from 30-40 μm were dispensed by the piezoelectric nozzle operating at 7 V and 30-60 Hz. The droplet on the surface was grown to ≈100 nL by accumulating the dispensed droplets and the advancing of the droplet contact line was recorded at 1 fps by an integrated CCD camera and custom optics. For droplets smaller than 100 nL, potential droplet resonance due to the addition of small dispensed droplets, relatively smaller than the size of the growing droplet, which may introduce a water hammer-type pressure and cause droplet wetting transition[80] was not present,[81] thus allowing for accurate measurements of contact angle during droplet dispensing. The receding contact angle was measured by stopping dispensing droplets and letting the droplet on the surface shrink *via* evaporation. The advancing and receding contact angles were extracted by a commercial software (FAMAS, Interface Measurements & Analysis System, Kyowa, Japan) *via*

the ellipse fit method. Measurements were repeated on 3-5 different locations on the surface to obtain the averaged advancing or receding contact angles (only in 3 locations for the nanowire CuO sealed sample). To monitor the surface contact angle variation with time, contact angles were measured multiple times during the surface exposure period. Contact angle measurements were conducted in the laboratory ambient air with temperature $T_a = 23 \pm 0.5°C$ and relative humidity $\Phi = 50 \pm 5\%$. Each measurement was accomplished within 20 min and samples were immediately returned to the designated exposure environment location to minimize the influence resulting from contact angle measurements.

To verify contact angle measurements and to obtain an 'equilibrium' macroscale contact angle, we used conventional goniometry to deposit 2 μL water droplets (OCA15Pro, Dataphysics). The macroscale contact angle measurements were in excellent agreement with the microscale results (Section S3, Figure S4, Supporting Information).

The roll-off angles were measured using a customized set-up consisting of a tilt stage, a digital inclinometer (MB5415-90, Meba) with an accuracy of 0.2º, a syringe pump (NE-300, New Era Pump Systems Inc.) along with a syringe capable of dispensing 6.6 ± 0.2 μL water droplets, and a camera (AMZT61BASIC, Canon) for capturing the rolling/sliding motion. During roll-off angle measurements, the sample was mounted on the tilt stage with an initial tilting angle of 0º (horizontal). The syringe tip was placed near the surface and water was gently dispensed onto the surface with an injection rate of ≈ 1 uL/s until the droplet reached the prescribed volume of 6.6 ± 0.2 μL. The syringe tip was gently removed from the droplet and the generated droplet was left to rest on the surface for ≈10 s, allowing for sufficient time for droplet wetting and equilibration. The tilting angle of the surface was then increased slowly with in increments of <0.5º until the droplet

started to slide or roll off the surface. The measurements were repeated on 10 locations on the surface to obtain a spatially averaged roll-off angle.

Scanning electron microscopy was performed on an SEM (Quanta 200 FEG, FEI, US) at an imaging voltage of 15 kV. Three-dimensional morphology of the laser-processed microstructures (Figure 1d) was imaged by a white-light interference profilometer (Zygo, NexView, US) using a 50X magnification lens.

To determine the surface chemistry, XPS measurements were performed at grazing (15°) and normal takeoff angles using a Kratos Axis ULTRA instrument (Kratos Analytical, Ltd., UK). The XPS data was analyzed using CasaXPS software (Casa software, Ltd., UK). To monitor the chemistry change with time, XPS measurements were performed on samples with exposure time of 0, 3, 14, and 194 days, with the 0-day-exposure sample being cleaned by plasma for 3-5 min at a medium power setting right before XPS measurements.

Time-of-Flight Secondary Ion Mass Spectroscopy (ToF-SIMS) was performed using a PHI TRIFT III system (PHI, US) in bunched mode for both positive and negative secondary ions detection. The suppressor voltage and emission current were 10 kV and 10-30 nA, respectively. The scanning area was 250 × 250 μm. The data were analyzed using WinCadence software (PHI, US).

Observation of Condensation Phenomena

The condensation behavior (Figure 5) on the different surfaces was observed by using a customized top-view setup consisting of an upright optical microscope (Eclipse LV100, Nikon) and a high-resolution camera (DS-Qi2, Nikon) for top-view analysis.[72] Samples were mounted horizontally on a cold stage (TP104SC-mk2000A, Instec, USA) which was cooled to T_s = 5.0 ±

0.5 °C to condense water vapor in laboratory ambient air with a temperature $T_a = 23 \pm 0.5$°C and relative humidity $\Phi = 50 \pm 5\%$ (RO120, Roscid Technologies, USA). Condensation behavior was recorded at 4 fps at 20-100× magnification. Illumination was supplied by an LED light source (SOLA SM II Light Engine, Lumencor). The LED light source was specifically chosen for its high-intensity, low-power consumption (2.5 W), and narrow spectral range (380−680 nm) in order minimize heat generation at the surface due to light absorption.

To observe the small droplets beneath the large droplets (Figure 5a), water vapor condensation on the horizontally mounted hierarchical CuO nanowire surface was allowed to proceed for > 20 min in order to form large droplets *via* droplet coalescence without gravitational shedding. The center of the microscope view field was adjusted to the center-of-mass of the large droplet and then the focal plane was shifted downwards through the large droplet.[82]

Side-View Droplet Jumping Imaging

To study coalescence-induced droplet jumping and to eliminate interference from multiple droplets, we interfaced a high-speed camera (Phantom v711, Vision Research) with a piezoelectric micro-goniometer (MCA-3, Kyowa Interface Science, Japan). The CuO nanowire sample was horizontally placed on a three-axis stage. Back illumination was supplied by an LED source (TSPA22x8, AITECSYSTEM). The piezoelectric dispenser was placed above our hierarchical surface with a dispenser-to-surface spacing ranging from 5 to 10 mm. To grow droplets on the substrate, the piezoelectric dispenser was turned on to generate monodisperse droplets with diameters of 30 - 40 μm. The droplets accumulated on the sample surface to form droplets with targeted sizes. The piezoelectric dispenser was controlled with voltage and frequency of 7 V and 10-100 Hz, respectively, with no droplet resonance observed under these operating conditions. A

custom cage was set up to screen external airflow disturbances to the droplet dispensing apparatus. Imaging was performed with a ≈ 25X magnification with a capture rate of 8,000 fps. Experiments were conducted in ambient conditions with a temperature T_a = 23 ± 0.5 °C and relative humidity Φ = 50 ± 5%. Additional details of the analysis method can be found in a separate paper.[83]

Plasma Modification

Air plasma (PDC-001-HP, Harrick Plasma, US) was used to clean and modify the CuO nanowire and CuO nanoblade surfaces. The plasma chamber was first vacuumed to < 27 Pa and then the samples were treated in the chamber with the air plasma for 3-5 min at a medium power setting. The effectiveness of the plasma cleaning was confirmed by the 0º apparent water contact angle measured using the microgoniometer immediately after the plasma treatment.

Organic Solvent Cleaning

To test the surface affinity to the adsorbed VOC molecules, we cleaned the CuO nanowire and CuO nanoblade surfaces with organic solvents. Samples that already reached saturated superhydrophobicity due to VOC adsorption were rinsed in acetone, isopropanol, ethanol, and DI water for 5 min, respectively, and then dried with clean nitrogen.

ASSOCIATED CONTENT

The authors declare no competing financial interest.

Supporting Information

The supporting information is available free of charge on the ACS Publication website at DOI: ##/###.

Further information about calculation of the jumping velocity of the coalescing droplets (Section S1), the non-flaking CuO nanowires fabrication (Section S2), surface characterization (Section S3), environmental condition characterization (Section S4), repeatability and universality of VOC-induced hydrophobicity (Section S5), surface chemistry analysis (Section S6), solar exposure tests, mechanical durability, thermal stability, self-healing tests (Section S7), condensation on other samples (Section S8), and adsorption kinetics model (Section S9) can be found on the accompanying Supporting Information (PDF).

Five videos showing small condensate droplets growing and disappearing beneath the large droplets (Video S1), coalescence-induced condensate droplet jumping under optical microscopy (Video S2), coalescence-induced condensate droplet jumping during pure vapor condensation (Video S3), coalescence and jumping dynamics of droplets under high-speed camera (Video S4), and droplet nucleation and growth on the CuO nanowires (Video S5), on hierarchical CuO nanowire surfaces.

Video S1 (AVI)

Video S2 (AVI)

Video S3 (AVI)

Video S4 (AVI)

Video S5 (AVI)

AUTHOR INFORMATION

Corresponding Authors

* E-mail: Xiao Yan: yan-x13@tsinghua.org.cn, Daniel Orejon: d.orejon@ed.ac.uk, Feng Chen: fengchen@tsinghua.edu.cn, Nenad Miljkovic: nmiljkov@illinois.edu

Author Contributions

X.Y., F.C., and N.M. conceived the initial idea for this research. N.M. guided the overall work. F.C. and Z.H. guided the surface fabrication. X.Y. F.C. and Z.H. fabricated and characterized the experimental samples. J.O., D.O., and H.C. carried out the XPS and ToF-SIMS measurements and analysis. X.Y., L.F., L.L, C.Z., and S.S. carried out the experiments. X.Y., H.C., D.O., J.O., and F.C. analyzed the data. X.Y. and N.M. carried out the theoretical analysis. All the authors were responsible for writing the paper and have given approval to the final version of the manuscript.

ACKNOWLEDGMENTS

J.O., H.C., and N.M acknowledge funding support from the Office of Naval Research (Grant No. N00014-16-1-2625). S.S. and N.M. gratefully acknowledge funding support from the National Science Foundation under Award No. 1554249. X.Y., F.C., and Z.H. gratefully acknowledge funding support from the National Natural Science Foundation of China (Grant No. 51206092) and National Science and Technology Major Project (ZX06901). X.Y. gratefully acknowledges funding support from China Scholarship Council (Grant No. 201606210181). N.M. and D.O. gratefully acknowledges funding support from the International Institute for Carbon Neutral Energy Research (WPI-I2CNER), sponsored by the Japanese Ministry of Education, Culture, Sports, Science, and Technology. D.O. acknowledges the support received from JSPS KAKENHI Grant No. JP18K13703. Laser etching and scanning electron microscopy were conducted in the School of Mechanical Engineering, Tsinghua University, with help from Xueqian Zhang, Lei Liu, and Guisheng Zou. Thermal oxidation was conducted at the Institute of Nuclear and New Energy Technology, Tsinghua University, with help from Gengyu Zhang and Mingfen Wen. X-ray

photoelectron spectroscopy and Time of Flight Secondary Ion Mass Spectroscopy were carried out in the Frederick Seitz Materials Research Laboratory Central Facilities, University of Illinois.

FIGURES

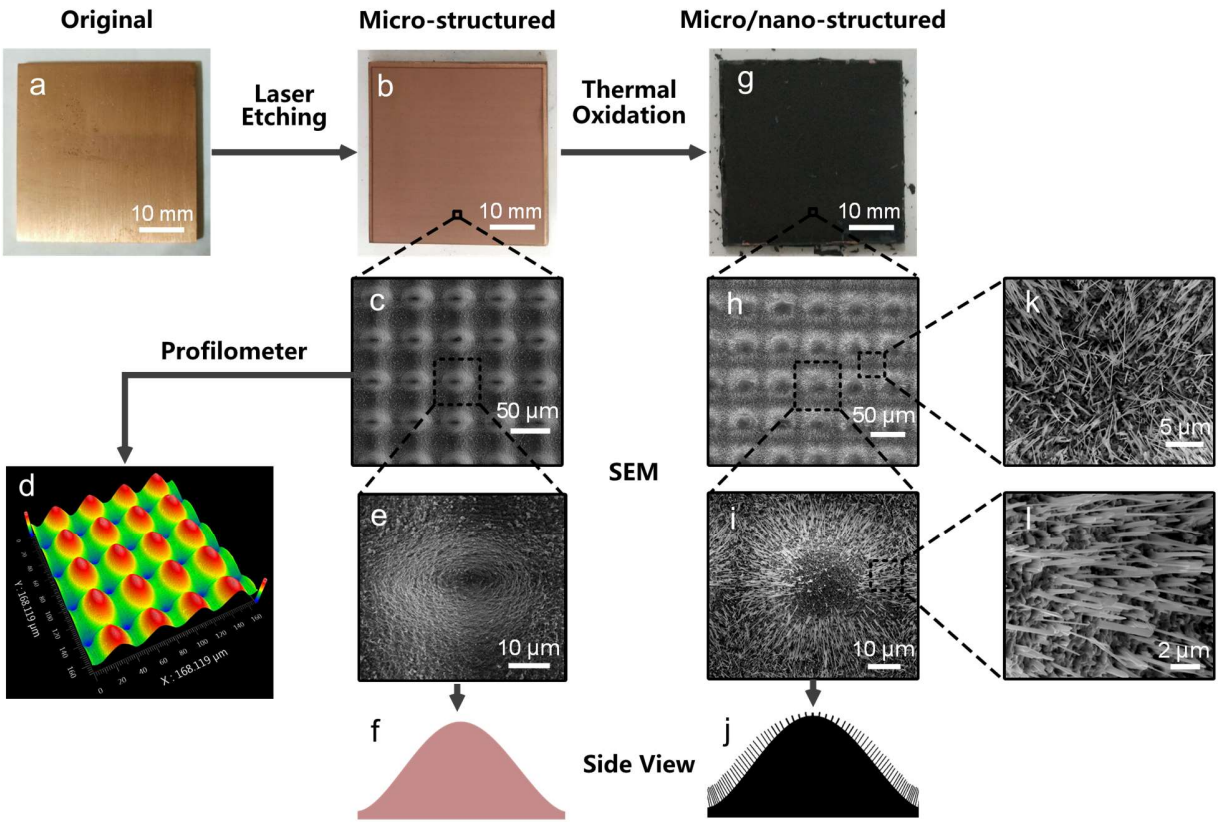

Figure 1. Photograph of the (a) original 40 × 40 × 2 mm Cu plate, and (b) laser-etched microstructured Cu plate. (c) Scanning electron microscopy (SEM) of the microstructures showing micro-bumps. (d) Three-dimensional (3D) morphology of the microstructured surface imaged by a white-light interference profilometer (Section S3, Figure S2, Supporting Information). (e) SEM of individual microstructures shown in (c). (f) Schematic of the side view of a single microstructure feature. (g) Photograph of the hierarchical micro/nano-structured surface immediately after oxidation. SEM images of (h) the hierarchical CuO nanowire surface and (i) an individual unit in (h). (j) Schematic of the side view of a single micro/nanostructured feature. High-resolution SEM images of the CuO nanowires residing (k) in the microstructure valleys and (l) on the microstructure sloped walls.

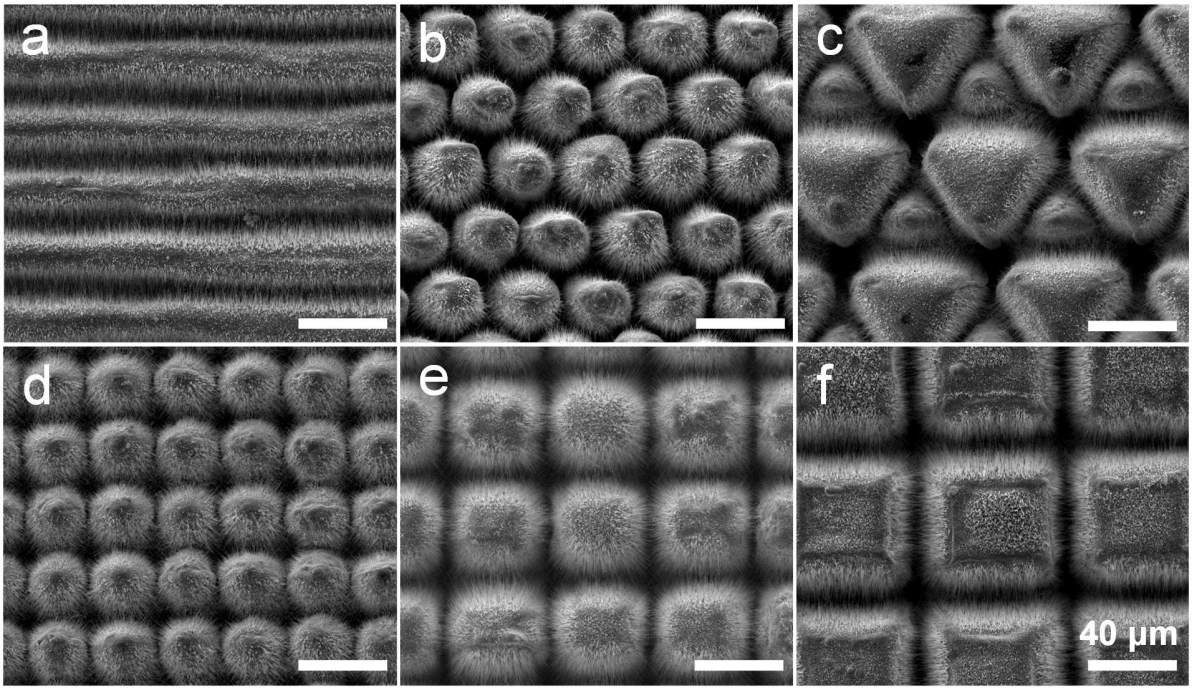

Figure 2. Scanning Electron Microscopy SEM of hierarchical CuO nanowire surfaces with controllable geometries. (a) Nanowire-covered grooves, (b) triangle-distributed cones, and (c) triangle columns were generated by changing the laser-scanning trajectory. By increasing the laser-scanning interval while fixing the trajectory pattern, (d-f) nanowire-covered hill-like microarrays with growing size or decreasing number density were obtained. The surfaces with hill-like structures (d-f) are selected in the subsequent studies given their merits regarding condensation performance. Scale bars are all 40 microns.

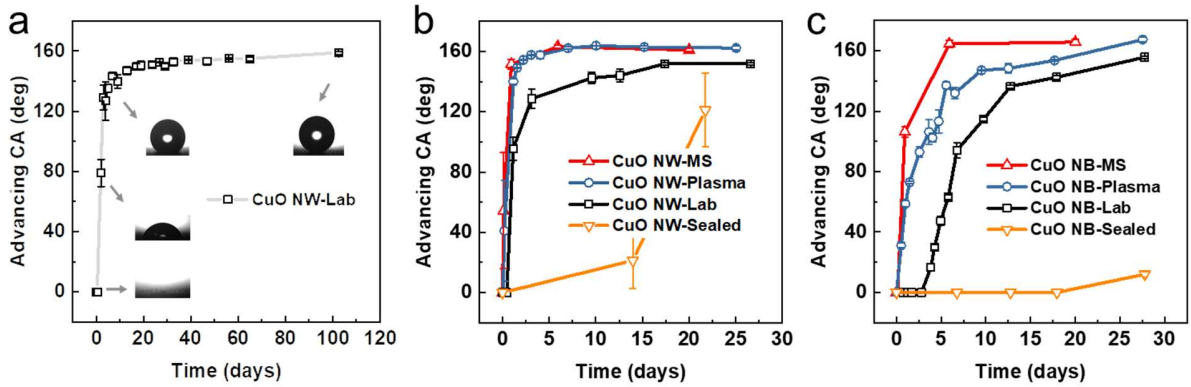

Figure 3. Water droplet apparent advancing contact angle as a function of time on (a and b) hierarchical CuO nanowire (CuO NW) and (c) CuO nanoblade (CuO NB) surfaces. (a) CuO NW exposed to laboratory environment (Lab, black ☐) in Urbana, USA, with long exposure time; (b) CuO NW exposed to machine shop (MS, red △), exposed to laboratory environment (Lab, black ☐), isolated in a container (Sealed, orange ▽), and air plasma modified CuO NW exposed to laboratory environment (Plasma, blue ○). (c) CuO NB exposed to machine shop (MS, red △), exposed to the laboratory environment (Lab, black ☐), isolated in a container (Sealed, orange ▽), and air plasma modified CuO NB exposed to the laboratory environment (Plasma, blue ○). See Methods for contact angle measurement details. The time $t = 0$ corresponds to the time when the samples were synthesized or modified with plasma. Both hierarchical CuO nanowire surfaces in (a) and (b) have the same microstructures with interval $I = 40$ μm and height $H \approx 50$ μm. All CuO nanoblade samples in (c) were fabricated at the same time with the same recipe (see Methods for fabrication details). Additional cycles of superhydrophilicity-to-superhydrophobicity transition and efficacy of plasma modification can be seen in Section S5 and Figure S8 of the Supporting Information. The measurement of initial zero apparent contact angles on the fresh samples is detailed in Section S3 of the Supporting Information.

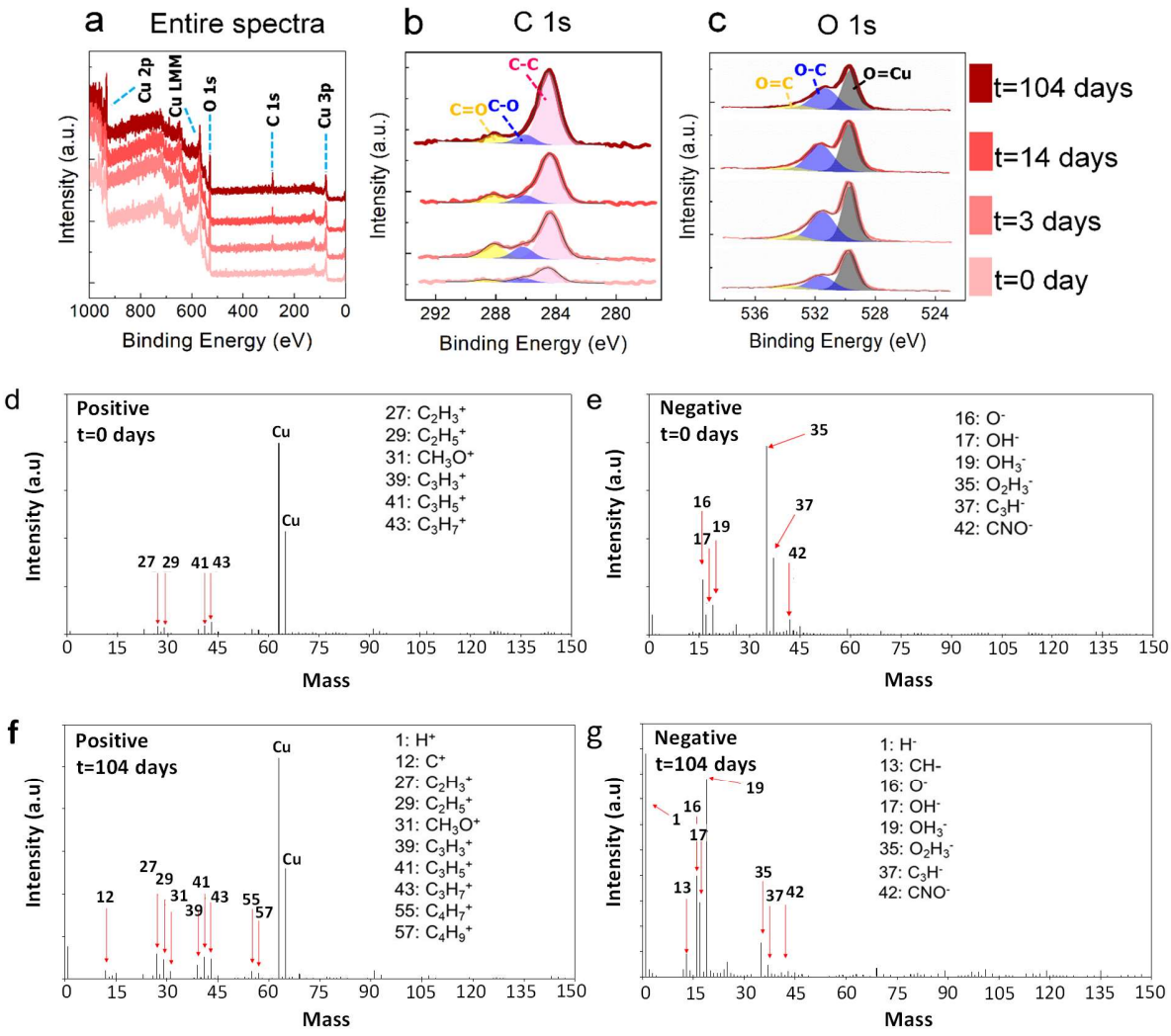

Figure 4. Time-resolved XPS and ToF-SIMS spectra of the hierarchical CuO nanowire surfaces. XPS spectra showing (a) broadband scan results, (b) high-resolution spectra for C 1s, and (c) high-resolution spectra for O 1s, at different exposure times: 0-day, 3-day, 14-day and 104-day. ToF-SIMS results of the (d) positive and (e) negative ion counts on clean hierarchical CuO nanowire surface, and (f) positive and (g) negative ion counts for atmospherically exposed CuO nanowire surface at 104-day exposure time. The surface for (d) and (e) was cleaned by air plasma for 3-5 min at a medium power setting (30 W).

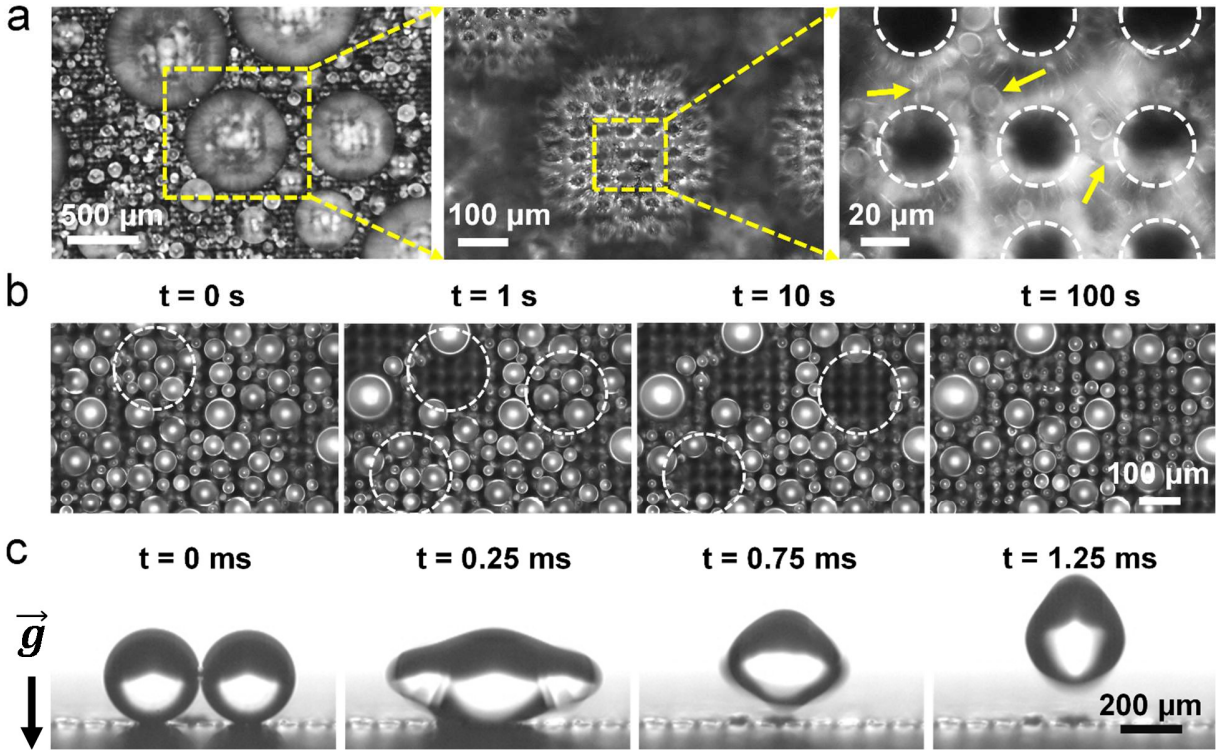

Figure 5. (a) Top-view optical microscopy images of atmospheric water vapor condensation on the VOC saturated (> 30 days, Urbana, IL USA) hierarchical CuO nanowire surface showing condensate droplets in the Cassie–Baxter state. Due to the absence of condensate removal by gravity (horizontal surface), large droplets accumulated for t > 20 minutes. Focal plane shift imaging revealed the presence of small droplets (identified with arrows) beneath larger droplets, signifying the suspended or partially wetting droplet morphology (see Video S1). (b) Top-view time-lapse optical microscopy images of coalescence-induced droplet jumping on the hierarchical CuO nanowire surface during atmospheric water vapor condensation (see Video S2). The gravitational vector points into the page for images in a and b. (c) Side-view high-speed time-lapse images of coalescence-induced droplet jumping of paired water droplets on the hierarchical CuO nanowire surface (see Video S4). Experimental conditions: in (a) and (b), surface temperature T_s = 5.0 ± 0.5°C, ambient air temperature T_a = 23 ± 0.5°C, and relative humidity Φ = 50 ± 5%; in (c), $T_s \approx T_a$ = 23 ± 0.5 °C and Φ = 50 ± 5%. Surface structure parameters: (a), microstructure interval I = 48 µm and microstructure height $H \approx$ 50 µm; (b) I = 40 µm and $H \approx$ 50 µm; and (c) I = 90 µm and $H \approx$ 50 µm.

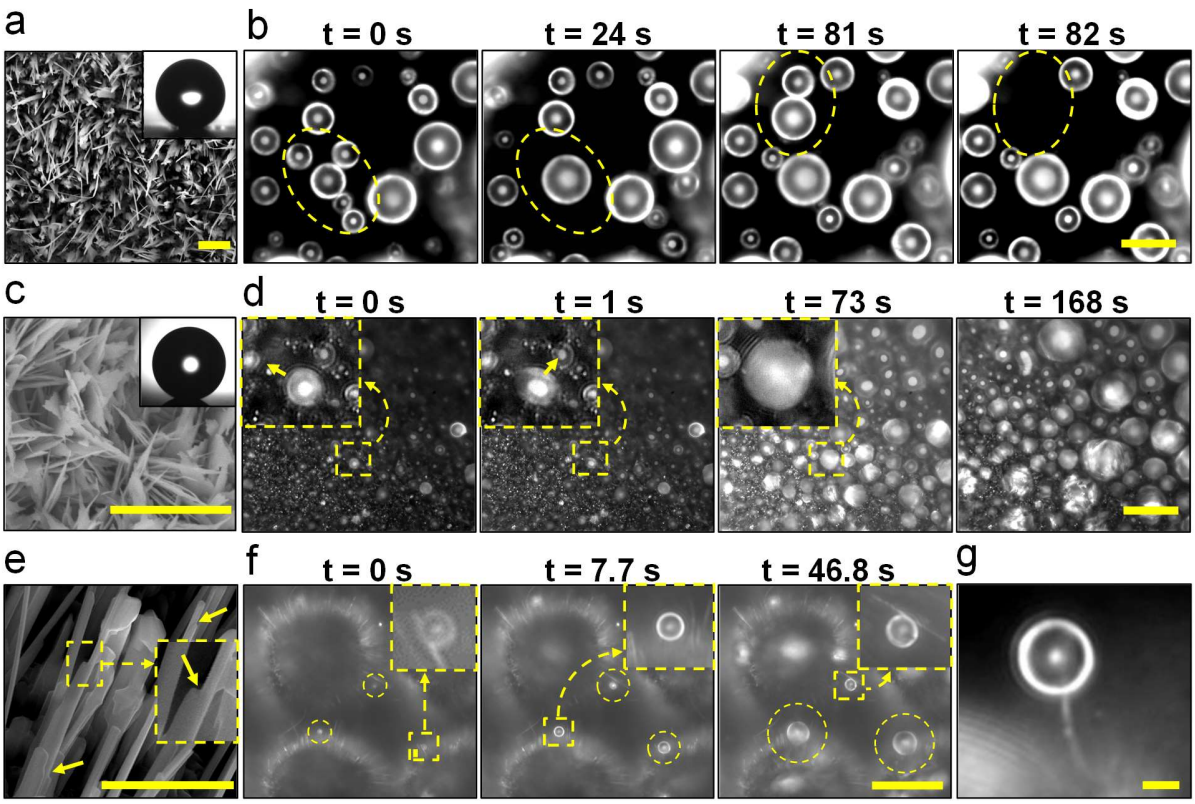

Figure 6. Nucleation, growth, and coalescence dynamics of condensate droplets on atmospheric-mediated (a, b) CuO nanowire and (c, d) CuO nanoblade surfaces. (b) On the CuO nanowire surface in (a), the condensate droplets (< 10 μm in radius) displayed a spherical morphology while growing in size and coalescing with neighboring droplets throughout condensation. Coalescence dynamics and coalescence-induced droplet jumping are outlined with dashed ellipses. In (a), a microstructure interval of I = 200 μm was chosen to minimize the effect of microscale structures and to focus on the nanotexture. Insets in (a) and (c) show the advancing apparent contact angles on the nanowire and nanoblade surfaces, which were 162 ± 2° and 167 ± 2°, respectively. Receding contact angles on the two surfaces were 145 ± 6° and 0°, respectively. (d) On the CuO nanoblade surface in (c), the droplets spread laterally as they grew and coalesced, as the contact line remained pinned. (e-g) Preferential nucleation on the CuO nanowire tips with characteristic concave step as shown in (e). (f) Droplet nucleating on tips and growing from radii 0.5 to 3.5 μm (see Video S5). (g) A condensate droplet with ≈ 2.1 μm radius supported by a single nanowire with thickness ≈ 200 nm. Condensation conditions: T_s = 5.0 ± 0.5°C, T_a = 23 ± 0.5°C, and Φ = 50 ± 5%. Experimental observations were carried out once the surfaces reached the saturated advancing contact angle in Urbana, IL USA. Scale bars: 2 μm in (a), (c), (e), and (g); 20 μm in (b), (d), and (f).

GRAPHICAL ABSTRACT

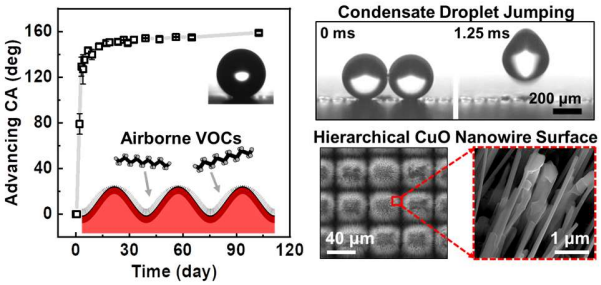

References

1. Wisdom, K. M.; Watson, J. A.; Qu, X.; Liu, F.; Watson, G. S.; Chen, C. H., Self-Cleaning of Superhydrophobic Surfaces by Self-Propelled Jumping Condensate. *Proc. Natl. Acad. Sci.* **2013**, 110, 7992-7997.
2. Rothstein, J.; Waterhouse, N.; Daniello, R., Drag Reduction in Turbulent Flows Over Superhydrophobic Surfaces. *Phys. Fluids* **2009**, 21, 85103.
3. Ghosh, A.; Ganguly, R.; Schutzius, T. M.; Megaridis, C. M., Wettability Patterning for High-Rate, Pumpless Fluid Transport On Open, Non-Planar Microfluidic Platforms. *Lab Chip* **2014**, 14, 1538-1550.
4. Zheng, S.; Li, C.; Fu, Q.; Xiang, T.; Hu, W.; Wang, J.; Ding, S.; Liu, P.; Chen, Z., Fabrication of a Micro-Nanostructured Superhydrophobic Aluminum Surface with Excellent Corrosion Resistance and Anti-Icing Performance. *RSC Adv.* **2016**, 6, 79389-79400.
5. Lv, J. Y.; Song, Y. L.; Jiang, L.; Wang, J. J., Bio-Inspired Strategies for Anti-Icing. *ACS Nano* **2014**, 8, 3152-3169.
6. Mouterde, T.; Lehoucq, G.; Xavier, S.; Checco, A.; Black, C. T.; Rahman, A.; Midavaine, T.; Clanet, C.; Quéré, D., Antifogging Abilities of Model Nanotextures. *Nat. Mater.* **2017**, 16, 658-663.
7. Miljkovic, N.; Enright, R.; Nam, Y.; Lopez, K.; Dou, N.; Sack, J.; Wang, E. N., Jumping-Droplet-Enhanced Condensation On Scalable Superhydrophobic Nanostructured Surfaces. *Nano Lett.* **2013**, 13, 179-187.
8. Cui, Y.; Paxson, A. T.; Smyth, K. M.; Varanasi, K. K., Hierarchical Polymeric Textures *Via* Solvent-Induced Phase Transformation: A Single-Step Production of Large-Area Superhydrophobic Surfaces. *Colloids Surf., A* **2012**, 394, 8-13.
9. Tuteja, A.; Choi, W.; Ma, M.; Mabry, J. M.; Mazzella, S. A.; Rutledge, G. C.; McKinley, G. H.; Cohen, R. E., Designing Superoleophobic Surfaces. *Science*, 5856, 1618-1622.
10. Quéré, D., Wetting and Roughness. *Annu. Rev. Mater. Res.* **2008**, 38, 71-99.
11. Attinger, D.; Frankiewicz, C.; Betz, A. R.; Schutzius, T. M.; Ganguly, R.; Das, A.; Kim, C.; Megaridis, C. M., Surface Engineering for Phase Change Heat Transfer: A Review. *MRS Energy Sustain. A Rev. J.* **2014**, 1, E4.
12. Maydanik, Y. F., Loop Heat Pipes. *Appl. Therm. Eng.* **2005**, 25, 635-657.
13. Nusselt, W., The Surface Condensation of Water Vapour. *VDI Z.* **1916**, 60, 541-546.
14. Rose, J. W., Dropwise Condensation Theory and Experiment: A Review. *J. Power Energy* **2002**, 216, 115-128.
15. Schmidt, E.; Schurig, W.; Sellschopp, W., Condensation of Water Vapour in Film and Drop Form. *Tech. Mech. Thermodyn.* **1930**, 1, 53-63.
16. Miljkovic, N.; Preston, D. J.; Enright, R.; Wang, E. N., Electric-Field-Enhanced Condensation On Superhydrophobic Nanostructured Surfaces. *ACS Nano* **2013**, 7, 11043-11054.
17. Miljkovic, N.; Preston, D. J.; Enright, R.; Wang, E. N., Electrostatic Charging of Jumping Droplets. *Nat. Commun.* **2013**, 4, 2517.
18. Miljkovic, N.; Enright, R.; Wang, E. N., Effect of Droplet Morphology On Growth Dynamics and Heat Transfer During Condensation On Superhydrophobic Nanostructured Surfaces. *ACS Nano* **2012**, 6, 1776-1785.
19. Boreyko, J. B.; Chen, C. H., Self-Propelled Dropwise Condensate On Superhydrophobic Surfaces. *Phys. Rev. Lett.* **2009**, 103, 184501.

20. Qu, X.; Boreyko, J. B.; Liu, F.; Agapov, R. L.; Lavrik, N. V.; Retterer, S. T.; Feng, J. J.; Collier, C. P.; Chen, C., Self-Propelled Sweeping Removal of Dropwise Condensate. *Appl. Phys. Lett.* **2015**, 106, 221601.
21. Paxson, A. T.; Yagüe, J. L.; Gleason, K. K.; Varanasi, K. K., Stable Dropwise Condensation for Enhancing Heat Transfer *Via* the Initiated Chemical Vapor Deposition (Icvd) of Grafted Polymer Films. *Adv. Mater.* **2014**, 26, 418-423.
22. Zhang, Y.; Zou, G.; Liu, L.; Zhao, Y.; Liang, Q.; Wu, A.; Zhou, Y. N., Time-Dependent Wettability of Nano-Patterned Surfaces Fabricated by Femtosecond Laser with High Efficiency. *Appl. Surf. Sci.* **2016**, 554-559.
23. Kietzig, A.; Hatzikiriakos, S. G.; Englezos, P., Patterned Superhydrophobic Metallic Surfaces. *Langmuir* **2009**, 25, 4821-4827.
24. Westwater, J. W., Gold Surfaces for Condensation Heat Transfer. *Gold Bull.* **1981**, 14, 95-101.
25. Chang, F.; Cheng, S.; Hong, S.; Sheng, Y.; Tsao, H., Superhydrophilicity to Superhydrophobicity Transition of CuO Nanowire Films. *Appl. Phys. Lett.* **2010**, 96, 114101.
26. Feng, X.; Feng, L.; Jin, M.; Zhai, J.; Jiang, L.; Zhu, D., Reversible Super-Hydrophobicity to Super-Hydrophilicity Transition of Aligned Zno Nanorod Films. *J. Am. Chem. Soc.* **2004**, 126, 62-63.
27. Tian, Y.; Jiang, L., Intrinsically Robust Hydrophobicity. *Nat. Mater.* **2013**, 12, 291-292.
28. Preston, D. J.; Miljkovic, N.; Sack, J.; Enright, R.; Queeney, J.; Wang, E. N., Effect of Hydrocarbon Adsorption On the Wettability of Rare Earth Oxide Ceramics. *Appl. Phys. Lett.* **2014**, 105, 11601.
29. Lundy, R.; Byrne, C.; Bogan, J.; Nolan, K.; Collins, M. N.; Dalton, E.; Enright, R., Exploring the Role of Adsorption and Surface State On the Hydrophobicity of Rare Earth Oxides. *ACS Appl. Mater. Interfaces* **2017**, 9, 13751-13760.
30. Azimi, G.; Dhiman, R.; Kwon, H.; Paxson, A. T.; Varanasi, K. K., Hydrophobicity of Rare-Earth Oxide Ceramics. *Nat. Mater.* **2013**, 12, 315-320.
31. Li, L. H.; Chen, Y., Superhydrophobic Properties of Nonaligned Boron Nitride Nanotube Films. *Langmuir* **2010**, 26, 5135-5140.
32. Boinovich, L. B.; Emelyanenko, A. M.; Pashinin, A. S.; Lee, C. H.; Drelich, J.; Yap, Y. K., Origins of Thermodynamically Stable Superhydrophobicity of Boron Nitride Nanotubes Coatings. *Langmuir* **2011**, 28, 1206-1216.
33. Preston, D. J.; Mafra, D. L.; Miljkovic, N.; Kong, J.; Wang, E. N., Scalable Graphene Coatings for Enhanced Condensation Heat Transfer. *Nano Lett.* **2015**, 15, 2902-2909.
34. Kim, G.; Gim, S.; Cho, S.; Koratkar, N.; Oh, I., Wetting-Transparent Graphene Films for Hydrophobic Water-Harvesting Surfaces. *Adv. Mater.* **2014**, 26, 5166-5172.
35. Long, J.; Zhong, M.; Fan, P.; Gong, D.; Zhang, H., Wettability Conversion of Ultrafast Laser Structured Copper Surface. *J. Laser Appl.* **2015**, 27, S29107.
36. Zhang, Q.; Xu, D.; Zhou, X.; Wu, X.; Zhang, K., *In Situ* Synthesis of CuO and Cu Nanostructures with Promising Electrochemical and Wettability Properties. *Small* **2014**, 10, 935-943.
37. Sindelarova, K.; Granier, C.; Bouarar, I.; Guenther, A.; Tilmes, S.; Stavrakou, T.; Müller, J. F.; Kuhn, U.; Stefani, P.; Knorr, W., Global Data Set of Biogenic VOC Emissions Calculated by the Megan Model Over the Last 30 Years. *Atmos. Chem. Phys.* **2014**, 14, 9317-9341.

38. Guo, H.; Ling, Z. H.; Cheng, H. R.; Simpson, I. J.; Lyu, X. P.; Wang, X. M.; Shao, M.; Lu, H. X.; Ayoko, G.; Zhang, Y. L.; Saunders, S. M.; Lam, S. H. M.; Wang, J. L.; Blake, D. R., Tropospheric Volatile Organic Compounds in China. *Sci. Total Environ.* **2017**, 574, 1021-1043.
39. McDonald, B. C.; de Gouw, J. A.; Gilman, J. B.; Jathar, S. H.; Akherati, A.; Cappa, C. D.; Jimenez, J. L.; Lee-Taylor, J.; Hayes, P. L.; McKeen, S. A.; Cui, Y. Y.; Kim, S. W.; Gentner, D. R.; Isaacman-VanWertz, G.; Goldstein, A. H.; Harley, R. A.; Frost, G. J.; Roberts, J. M.; Ryerson, T. B.; Trainer, M., Volatile Chemical Products Emerging as Largest Petrochemical Source of Urban Organic Emissions. *Science* **2018**, 359, 760-764.
40. Gligorovski, S.; Abbatt, J., An Indoor Chemical Cocktail. *Science* **2018**, 359, 632-633.
41. Jiang, X.; Herricks, T.; Xia, Y., Cuo Nanowires Can be Synthesized by Heating Copper Substrates in Air. *Nano Lett.* **2002**, 2, 1333-1338.
42. Fan, P.; Bai, B.; Long, J.; Jiang, D.; Jin, G.; Zhang, H.; Zhong, M., Broadband High-Performance Infrared Antireflection Nanowires Facilely Grown On Ultrafast Laser Structured Cu Surface. *Nano Lett.* **2015**, 15, 5988-5994.
43. Wang, Z. Y.; Liu, J. T.; Hirak, D. M.; Weckman, D. C.; Kerr, H. W., Determining the Spot Size and Gaussian Distribution Coefficient of Pulsed Laser Beams Using Kapton Films. *J. Laser Appl.* **1993**, 1, 5-12.
44. Yuan, L.; Wang, Y. Q.; Mema, R.; Zhou, G. W., Driving Force and Growth Mechanism for Spontaneous Oxide Nanowire Formation During the Thermal Oxidation of Metals. *Acta Mater.* **2011**, 59, 2491-2500.
45. Clarke, D. R., Stress Generation During High-Temperature Oxidation of Metallic Alloys. *Curr. Opin. Solid State Mater. Sci.* **2002**, 3, 237-244.
46. Evans, A. G.; Crumley, G. B.; Demaray, R. E., On the Mechanical Behavior of Brittle Coatings and Layers. *Oxid. Met.* **1983**, 5-6, 193-216.
47. Mumm, F.; Sikorski, P., Oxidative Fabrication of Patterned, Large, Non-Flaking Cuo Nanowire Arrays. *Nanotechnology* **2011**, 22, 105605.
48. Zhang, Q.; Xu, D.; Hung, T. F.; Zhang, K., Facile Synthesis, Growth Mechanism and Reversible Superhydrophobic and Superhydrophilic Properties of Non-Flaking Cuo Nanowires Grown From Porous Copper Substrates. *Nanotechnology* **2013**, 24, 65602.
49. Balajka, J.; Hines, M. A.; DeBenedetti, W.; Komora, M.; Pavelec, J.; Schmid, M.; Diebold, U., High-Affinity Adsorption Leads to Molecularly Ordered Interfaces On Tio2 in Air and Solution. *Science* **2018**, 361, 786-789.
50. Yang, Z.; Liu, X.; Tian, Y., Insights Into the Wettability Transition of Nanosecond Laser Ablated Surface Under Ambient Air Exposure. *J. Colloid Interface Sci.* **2019**, 533, 268-277.
51. Long, J.; Zhong, M.; Zhang, H.; Fan, P., Superhydrophilicity to Superhydrophobicity Transition of Picosecond Laser Microstructured Aluminum in Ambient Air. *J. Colloid Interface Sci.* **2015**, 441, 1-9.
52. Long, J.; Fan, P.; Zhong, M.; Zhang, H.; Xie, Y.; Lin, C., Superhydrophobic and Colorful Copper Surfaces Fabricated by Picosecond Laser Induced Periodic Nanostructures. *Appl. Surf. Sci.* **2014**, 311, 461-467.
53. Wang, G.; Cheng, S.; Wei, W.; Zhou, Y.; Yao, S.; Zhang, H., Characteristics and Source Apportionment of Vocs in the Suburban Area of Beijing, China. *Atmos. Pollut. Res.* **2016**, 7, 711-724.

54. Hillborg, H.; Ankner, J. F.; Gedde, U. W.; Smith, G. D.; Yasuda, H. K.; Wikstr M, K.; Polymerteknologi; KTH; Institutioner, T., Crosslinked Polydimethylsiloxane Exposed to Oxygen Plasma Studied by Neutron Reflectometry and Other Surface Specific Techniques. *Polymer* **2000**, 41, 6851-6863.
55. Liston, E. M., Plasma Treatment for Improved Bonding: A Review. *J. Adhes.* **1989**, 30, 199-218.
56. Chen, C.; Cai, Q.; Tsai, C.; Chen, C.; Xiong, G.; Yu, Y. ô. R. Z., Dropwise Condensation On Superhydrophobic Surfaces with Two-Tier Roughness. *Appl. Phys. Lett.* **2007**, 75, 173108.
57. Rykaczewski, K.; Osborn, W. A.; Chinn, J.; Walker, M. L.; Scott, J. H. J.; Jones, W.; Hao, C.; Yao, S.; Wang, Z., How Nanorough is Rough Enough to Make a Surface Superhydrophobic During Water Condensation? *Soft Matter* **2012**, 8, 8786.
58. Miljkovic, N.; Wang, E. N., Condensation Heat Transfer On Superhydrophobic Surfaces. *MRS Bull.* **2013**, 38, 397-406.
59. Cassie, A. B. D.; Baxter, S., Wettability of Porous Surfaces. *Trans. Faraday Soc.* **1944**, 40, 546-551.
60. Enright, R.; Miljkovic, N.; Sprittles, J.; Nolan, K.; Mitchell, R.; Wang, E. N., How Coalescing Droplets Jump. *ACS Nano* **2014**, 8, 10352-10362.
61. Kim, M.; Cha, H.; Birbarah, P.; Chavan, S.; Zhong, C.; Xu, Y.; Miljkovic, N., Enhanced Jumping-Droplet Departure. *Langmuir* **2015**, 31, 13452-13466.
62. Bico, J.; Thiele, U.; Quéré, D., Wetting of Textured Surfaces. *Colloids Surf., A* **2002**, 206, 41-46.
63. Feng, L.; Zhang, Y.; Xi, J.; Zhu, Y.; Wang, N.; Xia, F.; Jiang, L., Petal Effect: a Superhydrophobic State with High Adhesive Force. *Langmuir* **2008**, 24, 4114-4119.
64. Wenzel, R. N., Resistance of Solid Surfaces to Wetting by Water. *Ind. Eng. Chem.* **1936**, 8, 988-994.
65. Grassian, V. H., When Size Really Matters: Size-Dependent Properties and Surface Chemistry of Metal and Metal Oxide Nanoparticles in Gas and Liquid Phase Environments. *J. Phys. Chem. C* **2008**, 112, 18303-18313.
66. Zhang, H.; Penn, R. L.; Hamers, R. J.; Banfield, J. F., Enhanced Adsorption of Molecules On Surfaces of Nanocrystalline Particles. *J. Phys. Chem. B* **1999**, 103, 4656-4662.
67. Hansen, B. J.; Chan, H. I.; Lu, J.; Lu, G.; Chen, J., Short-Circuit Diffusion Growth of Long Bi-Crystal Cuo Nanowires. *Chem. Phys. Lett.* **2011**, 504, 41-45.
68. Xu, W.; Lan, Z.; Peng, B.; Wen, R.; Ma, X., Heterogeneous Nucleation Capability of Conical Microstructures for Water Droplets. *RSC Adv.* **2015**, 5, 812-818.
69. Orejon, D.; Shardt, O.; Waghmare, P. R.; Kumar Gunda, N. S.; Takata, Y.; Mitra, S. K., Droplet Migration During Condensation On Chemically Patterned Micropillars. *RSC Advances* **2016**, 6, 36698-36704.
70. Wen, R.; Li, Q.; Wu, J.; Wu, G.; Wang, W.; Chen, Y.; Ma, X.; Zhao, D.; Yang, R., Hydrophobic Copper Nanowires for Enhancing Condensation Heat Transfer. *Nano Energy* **2017**, 33, 177-183.
71. Mulroe, M. D.; Srijanto, B. R.; Ahmadi, S. F.; Collier, C. P.; Boreyko, J. B., Tuning Superhydrophobic Nanostructures to Enhance Jumping-Droplet Condensation. *ACS nano* **2017**, 8, 8499-8510.
72. Cha, H.; Xu, C.; Sotelo, J.; Chun, J. M.; Yokoyama, Y.; Enright, R.; Miljkovic, N., Coalescence-Induced Nanodroplet Jumping. *Phys. Rev. Fluids* **2016**, 6, 64102.

73. Takeda, S.; Fukawa, M.; Hayashi, Y.; Matsumoto, K., Surface Oh Group Governing Adsorption Properties of Metal Oxide Films. *Thin Solid Films* **1999**, 1-2, 220-224.
74. Holden, K. M.; Wanniarachchi, A. S.; Marto, P. J.; Boone, D. H.; Rose, J. W., The Use of Organic Coatings to Promote Dropwise Condensation of Steam. *J. Heat Transfer* **1987**, 3, 768-774.
75. Woodruff, D. W.; Westwater, J. W., Steam Condensation On Electroplated Gold: Effect of Plating Thickness. *Int. J. Heat Mass Transfer* **1979**, 4, 629-632.
76. Cha, H.; Wu, A.; Kim, M.; Saigusa, K.; Liu, A.; Miljkovic, N., Nanoscale-Agglomerate-Mediated Heterogeneous Nucleation. *Nano Lett.* **2017**, 17, 7544-7551.
77. Wang, G.; Zhang, T., Oxygen Adsorption Induced Superhydrophilic-to-Superhydrophobic Transition On Hierarchical Nanostructured Cuo Surface. *J. Colloid Interface Sci.* **2012**, 377, 438-441.
78. Li, Z.; Wang, Y.; Kozbial, A.; Shenoy, G.; Zhou, F.; McGinley, R.; Ireland, P.; Morganstein, B.; Kunkel, A.; Surwade, S. P.; Li, L.; Liu, H., Effect of Airborne Contaminants On the Wettability of Supported Graphene and Graphite. *Nat. Mater.* **2013**, 12, 925-931.
79. Fan, P.; Zhong, M.; Bai, B.; Jin, G.; Zhang, H., Large Scale and Cost Effective Generation of 3D Self-Supporting Oxide Nanowire Architectures by a Top-Down and Bottom-Up Combined Approach. *RSC Adv.* **2016**, 6, 45923-45930.
80. Kwon, H. M.; Paxson, A. T.; Varanasi, K. K.; Patankar, N. A., Rapid Deceleration-Driven Wetting Transition During Pendant Drop Deposition On Superhydrophobic Surfaces. *Phys. Rev. Lett.* **2011**, 106, 36102.
81. Günay, A. A.; Sett, S.; Oh, J.; Miljkovic, N., Steady Method for the Analysis of Evaporation Dynamics. *Langmuir* **2017**, 33, 12007-12015.
82. Cha, H.; Chun, J. M.; Sotelo, J.; Miljkovic, N., Focal Plane Shift Imaging for the Analysis of Dynamic Wetting Processes. *ACS Nano* **2016**, 10, 8223-8232.
83. Yan, X.; Zhang, L.; Sett, S.; Feng, L.; Zhao, C.; Huang, Z.; Vahabi, H.; Kota, A. K.; Chen, F.; Miljkovic, N., Droplet Jumping: Effects of Droplet Size, Surface Structure, Pinning, and Liquid Properties. *ACS Nano* **2019**, 13, 1309-1323.